Geomorphology 122 (2010) 65–77

Contents lists available at ScienceDirect

Geomorphology

journal homepage: www.elsevier.com/locate/geomorph

Spatial and temporal variability in denudation across the Bolivian Andes from multiple geochronometers

Nadja Insel [a,*], Todd A. Ehlers [a,1], Mirjam Schaller [a,1], Jason B. Barnes [a,2], Sohrab Tawackoli [b], Christopher J. Poulsen [a]

[a] Department of Geological Sciences, University of Michigan, Ann Arbor, MI 48109-1005, USA
[b] Deutsche Gesellschaft für Technische Zusammenarbeit (GTZ), Casilla 8408, La Paz, Bolivia

ARTICLE INFO

Article history:
Received 19 August 2009
Received in revised form 12 May 2010
Accepted 17 May 2010
Available online 2 June 2010

Keywords:
Cosmogenic radionuclides
Denudation
Climate change
Morphology
Central Andes

ABSTRACT

We quantify spatial and temporal variations in denudation rates across the central Andean fold-thrust belt in Bolivia with particular focus on the Holocene. Measured and predicted ^{10}Be cosmogenic radionuclide (CRN) concentrations in river sediments are used to (1) calculate catchment-averaged denudation rates from 17 basins across two transects at different latitudes, and (2) evaluate the sensitivity of Holocene climate change on the denudation history recorded by the CRN data. Estimated denudation rates vary by two orders of magnitude from 0.04 to 1.93 mm yr^{-1} with mean values of 0.40 ± 0.29 mm yr^{-1} in northern Bolivia and 0.51 ± 0.50 mm yr^{-1} in the south. Results demonstrate no statistically significant correlation between denudation rates and morphological parameters such as relief, slope or drainage basin size. In addition, the CRN-derived denudation rates do not reflect present-day latitudinal variations in precipitation. Comparison to ~130 previously published denudation rates calculated over long (thermochronology-derived; >10^6 yrs), medium (CRN-derived; 10^2–10^4 yrs), and short timescales (sediment flux-derived; 10^1 yrs) indicate temporal variations in denudation rates that increase between 0 and 200% over the last ~5 ka. CRN modeling results suggest that the CRN-derived denudation rates may not be fully adjusted to wetter climate conditions recorded in the central Andes since the mid-Holocene. We conclude that large spatial variability in CRN denudation may be due to local variations in tectonics (e.g. faulting), while large temporal variability in denudation may be due to temporal variations in climate.

1. Introduction

A close link between tectonics, climate, and denudation in the evolution of mountain belts has been hypothesized in a variety of modeling and observational studies (e.g. Willett, 1999; Leturmy et al., 2000; Beaumont et al., 2001; Hilley and Strecker, 2004). For example, it has been proposed that regional variations in climate may strongly influence spatial variations in denudation, thereby affecting the style and location of deformation and exhumation (e.g. Willett, 1999). The 8000-km long Andes Mountains in South America are thought to exemplify these linkages because correlations between latitudinal variations in tectonic deformation, topography, and precipitation as well as denudation rate estimates suggest that climate-driven denudation exerts a fundamental control on mountain evolution (e.g. Masek et al., 1994; Montgomery et al., 2001). In particular, the central Andean fold-thrust belt (~14–26°S) is characterized by high relief and steep slopes north of 18°S that have been hypothesized to reflect high orographic precipitation and high denudation rates, while the more gentle and wider topography of the drier regions south of 18°S may reflect a tectonic landform less modified by climate and denudation (Masek et al., 1994; Horton, 1999; Barnes and Pelletier, 2006; McQuarrie et al., 2008b). Improved quantification of the spatial and temporal variations in magnitude and mechanism of denudation across the central Andes reveals variations in denudation processes that might be related to changes in tectonics, climate, or land use, and is essential to understand the role of denudation in shaping landscapes (Gillis et al., 2006; Barnes and Ehlers, 2009).

Terrestrial denudation rates are sensitive to both tectonics and climate, but the importance of each effect is difficult to constrain. Averaged long-term (>10^6 yrs) denudation rates in the Bolivian Andes that are estimated from low-temperature thermochronology (e.g. apatite fission track (AFT) dating) mainly represent denudation driven by tectonic-related processes and are similar along strike (Benjamin et al., 1987; Barnes et al., 2006; Gillis et al., 2006; Safran et al., 2006; Ege et al., 2007; Barnes et al., 2008; McQuarrie et al., 2008a). Averaged medium-term (10^2–10^4 yrs) denudation rates calculated from cosmogenic radionuclides (CRN) in the northern

* Corresponding author. Tel.: +1 734 764 5636; fax: +1 734 763 4690.
E-mail address: nadinsel@umich.edu (N. Insel).
[1] Now at Institut für Geowissenschaften, Universität Tübingen, Tübingen, D-72074, Germany.
[2] Now at Department of Geological Sciences, University of North Carolina, Chapel Hill, NC 27599-3315.

0169-555X/$ – see front matter
doi:10.1016/j.geomorph.2010.05.014

Bolivian Andes are within the range of long-term denudation rates in the same area (Safran et al., 2005). No medium-term denudation data exist from the southern part of the Bolivian Andes. Short-term (10^1–10^2 yrs) denudation rate estimates from sediment flux data in the Bolivian Andes mirror the present-day latitudinal precipitation gradient and indicate a disparity with ~3 times higher mean denudation rates in northern Bolivia (14–18°S) compared to the south (18–22°S) (Barnes and Pelletier, 2006). Previous studies suggest that the along-strike variability in denudation existed throughout the Holocene with an increase in denudation and north-south contrast since as early as the late Miocene (~10 Ma) (Anders et al., 2002; Safran et al., 2005; Barnes and Pelletier, 2006). Structural and thermochronometer data and basin sedimentation histories were used to infer orographically controlled and/or South American monsoon system-related intensification of precipitation and denudation in Bolivia also in the late Miocene (McQuarrie et al., 2008b; Uba et al., 2009). This intensification could be due to plateau uplift beyond some substantial elevation threshold (Garzione et al., 2006; Ehlers and Poulsen, 2009; Insel et al., 2009; Mulch et al., 2010).

In this study, we integrate 17 new cosmogenic ^{10}Be analyses with 43 previously published CRN data (Safran et al., 2005) to quantify catchment-averaged denudation rates from the Andean fold-thrust belt in Bolivia (Fig. 1a). New samples were collected across two different transects in the northern (~15ºS) humid and southern (~19ºS) dry part of the Bolivian Andes (Fig. 1b) with a focus on the Subandes which have been uplifted since the Miocene (e.g. Barnes et al., 2008; Uba et al., 2009). These data are used to quantify (1) spatial variations in denudation by comparing CRN-derived denudation rates from the northern and southern transects, and (2) temporal variations in denudation rates by comparing rates on different time scales. In addition, we (3) compare magnitudes of denudation with modern variations in precipitation and geomorphic indices (e.g. slope and relief). Our results complement previous work in the northern Bolivian Andes (Safran et al., 2005) and add new data from the southern Bolivian Andes to verify the strong disparity in denudation rates over time. The combination of our results with previously estimated sediment flux-derived denudation rates (Aalto et al., 2006; Barnes and Pelletier, 2006) reveal Holocene variations in denudation processes and the possible effect of climate change on radionuclide concentrations over the last ~5 ka.

2. Geologic, geomorphic, and climate setting

The central Andes (14–26ºS) form the widest and highest portion of the Andean Cordillera. The central Andean fold-thrust belt occupies the eastern flank of the Cordillera and is divided into four physiographic units (Fig. 1a; Kley et al., 1996; McQuarrie, 2002): (a) the low relief, internally-drained Altiplano (AP) with an average elevation of >3 km; (b) the structurally bivergent, high elevation Eastern Cordillera (EC); (c) the Interandean zone (IA); and (d) the tectonically active Subandes (SA). The thrust belt is the result of Cenozoic crustal shortening and thickening related to subduction of the Nazca plate below the South American plate (e.g. Isacks, 1988; Sempere et al., 1990; Allmendinger et al., 1997; Jordan et al., 1997; Kley and Monaldi, 1998; Oncken et al., 2006).

The central Andes are characterized by significant along-strike contrasts in the morphology and the style of deformation that have been ascribed to strong latitudinal changes in climate and/or tectonics (Fig. 1) (Isacks, 1988; Masek et al., 1994; Allmendinger et al., 1997; Horton, 1999; Montgomery et al., 2001). The high relief and narrow fold-thrust belt in the northern portion of the Bolivian Andes (~14–18°S) is distinctive from the wide and smooth topography in the south (~18–22°S). Based on cross-section balancing and low-temperature thermochronology, the average vertical exhumation over the last 20 Ma is higher (4–9 km) in the north than in the south (3–6 km) (e.g. Barnes et al., 2006, 2008; McQuarrie et al., 2008b).

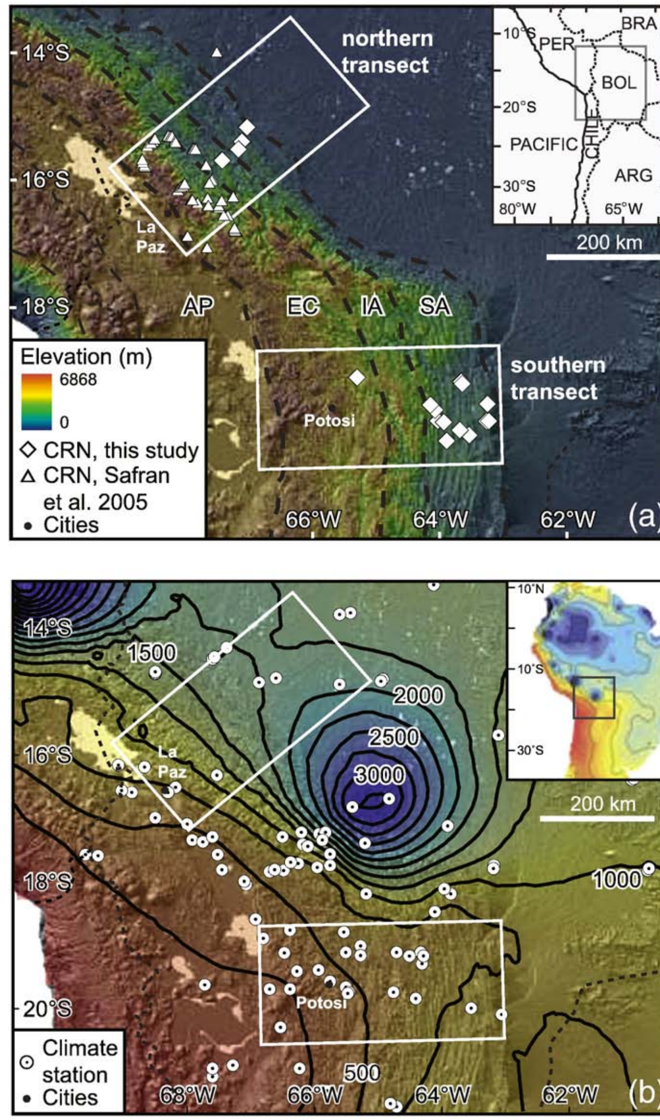

Fig. 1. Topography, precipitation, and cosmogenic radionuclide (CRN) samples of the Bolivian Andes. (a) Shaded 90 m digital elevation model (SRTM DEM) of the Bolivian Andes showing major morphological units (AP: Altiplano, EC: Eastern Cordillera, IA: Interandean zone, SA: Subandes) and location of study area transects. CRN samples are from this study (diamonds) and Safran et al. (2005) (triangles). Small dashed lines are country borders. Elevations span ~300–500 m in the foreland to 6800 m west of the AP. Inset shows study area location in west-central South America (modified from Barnes et al., 2008). (b) Same map showing modern precipitation distribution interpolated from the Global Historical Climatology Network climate station data (Peterson and Vose, 1997). Contour interval is 250 mm yr^{-1}. Inset shows 500 mm yr^{-1} precipitation contours for South America.

Lithologies involved in the deformation and exposed today are similar north to south, ranging from Ordovician to Devonian marine siliciclastic rocks and Carboniferous to Cretaceous non-marine clastics to Cenozoic synorogenic sediments (e.g. Sempere, 1995; Sempere et al., 1997; Horton, 1998; McQuarrie, 2002). As addressed in the discussion section, the mechanical strength of these sedimentary rocks in the study area is also similar along strike (McQuarrie and Davis, 2002) implying no latitudinal variation in erodibility of the different lithologies.

The central Andes are characterized by both latitudinally and orographically enhanced changes in precipitation (e.g. Aceituno, 1988; Garreaud and Wallace, 1997; Garreaud, 2000). The large-scale atmospheric circulation over South America leads to a strong regional precipitation gradient with up to 4 m yr^{-1} rainfall north of ~18°S and less than 1 m yr^{-1} south of 18°S (Fig. 1b). In addition, the central

Table 1
Cosmogenic sample locations, drainage basin statistics and information for CRN-derived, basin-averaged denudation rate estimates from the central Andes in Bolivia.

Sample ID	River	Sampled latitude (°S)	Sampled longitude (°W)	Sampled altitude (m)	Drainage (km^2)	Fm age[a]	Quartz yield (%)[b]	Mean relief (m)[c]	Mean slope (%)	Mean annual precipitation (mm yr^{-1})	Mean latitude (°S)	Mean altitude (m)	Production rate (atoms $(g_{(qtz)}\ yr)^{-1}$)[d]		^{10}Be conc (10^4atoms $g_{(qtz)}^{-1}$)[e]	^{26}Al conc (10^4atoms $g_{(qtz)}^{-1}$)[e]	Denudation rate (mm yr^{-1})[f]	Apparent age (kyr)
Northern transect																		
N02	Rio Yucumo	15.16	67.04	263	48	Dv-Te	79	460	24	1669	15.18	618	5.26		0.52 ± 0.06		0.83 ± 0.11	0.99
N04	Rio Quiquibey	15.39	67.12	595	332	Cb	66	425	23	1678	15.50	1106	7.58	46.15	3.64 ± 0.18	17.23 ± 3.70	0.17 ± 0.01	4.80
N04[g]		15.39	67.12	595							15.50	1106	7.58	46.15	3.47 ± 0.12		0.18 ± 0.01	4.57
N05	Rio Inicua	15.51	67.17	562	205	Te	34	494	23	1648	15.55	1027	7.19	43.82	5.11 ± 0.35	31.68 ± 4.73	0.11 ± 0.01	7.10
N06	Rio Pequende	15.68	67.43	840	34	Dv	50	645	33	1502	15.71	1397	9.40	57.27	5.47 ± 0.21	23.82 ± 3.68	0.14 ± 0.01	5.82
N06[g]		15.68	67.43	840							15.71	1397	9.40	57.27	2.77 ± 0.15		0.24 ± 0.02	3.43
Southern transect																		
S01[g]	Rio El Chaleno	19.79	63.26	871	4	Cb-Me	73	414	41	767	19.80	1119	7.98		2.09 ± 0.22		0.31 ± 0.04	2.62
S03[g]	Rio Bateon	19.79	64.03	1246	5	Dv	82	521	32	727	19.77	1504	10.57		0.96 ± 0.05		0.90 ± 0.06	0.91
S04	Rio Azero	19.61	64.08	1101	3763	Sil-Dv	53	621	30	670	19.67	2250	18.02		13.69 ± 0.38		0.11 ± 0.01	7.59
S04[g]		19.61	64.08	1101							19.67	2250	18.02		7.16 ± 0.11		0.20 ± 0.01	3.98
S05	Rio Canas	19.53	64.15	1374	7	Dv	26	820	41	688	19.56	2059	15.49		28.86 ± 0.84		0.04 ± 0.003	18.63
S05[g]		19.53	64.15	1374							19.56	2059	15.49		24.72 ± 2.74		0.05 ± 0.006	15.96
S06[g]	Rio Cachu Mayu	19.10	65.30	2499	1318	Me/Ord	62	514	26	581	18.92	3515	36.16		73.47 ± 2.88		0.04 ± 0.003	20.32
S08	Rio Saipuru	19.52	63.25	832	129	Cb-Te	85	378	19	760	19.52	1082	7.75	47.20	1.63 ± 0.13	5.85 ± 2.36	0.39 ± 0.04	2.10
S09	Rio Charagua	19.79	63.23	830	152	Cb-Te	86	435	21	765	19.75	1125	8.03	48.94	1.56 ± 0.13	5.29 ± 2.96	0.42 ± 0.04	1.95
S09[g]		19.79	63.23	830							19.75	1125	8.03	48.94	1.60 ± 0.28		0.41 ± 0.07	2.00
S10	Rio Parapeti	20.01	63.54	789	5194	Dv-Te	70	446	24	748	20.13	1437	10.56	64.30	3.02 ± 0.17	10.82 ± 3.41	0.28 ± 0.02	2.86
S11	Rio Iviyeca	19.93	63.68	989	20	(Dv-)Te	54	561	31	753	19.92	1298	9.15		1.14 ± 0.11		0.65 ± 0.07	1.25
S12	Rio Banado	20.10	63.89	988	1036	Dv-Te	83	379	20	741	19.92	1329	9.41	57.32	2.62 ± 0.15	13.38 ± 3.25	0.29 ± 0.02	2.78
S13	Rio Zapaltar	19.80	63.94	1115	52	Dv-Te	77	451	25	729	19.75	1374	9.66		1.04 ± 0.09		0.75 ± 0.07	1.08
S15	Rio Nancahuazu	19.17	63.66	532	3127	Dv-Te	82	342	18	742	19.54	1072	7.74	47.15	1.29 ± 0.09	4.65 ± 3.08	0.49 ± 0.04	1.66
S16	Rio Saladille	19.20	63.65	575	47	Cb-Me	80	402	23	734	19.22	842	6.46		0.27 ± 0.05		1.93 ± 0.36	0.42

[a] Fm age: formation age; Ord Ordovician; Sil Silurian; Dv Devonian; Cb Carboniferous; Me Mesozoic; Te Tertiary.
[b] Quartz content derived from the sample material (e.g. amount of quartz in relation to other minerals within the sample).
[c] Relief is calculated by substracting the highest and lowest elevations within a circular neighborhood with 2 km in radius.
[d] Production rate is scaled to lat and lon, and corrected for topographic shielding, first value is for ^{10}Be, second value for ^{26}Al, no correction necessary for snow coverage or thickness.
[e] Error on concentrations includes analytical uncertainties.
[f] Denudation rate based on ^{10}Be concentration; total error includes analytical uncertainties and calculated uncertainties for production rate that is based on an assumed 10 percent uncertainty in calculated mean altitude and size of the upstream catchment area.
[g] Grain size: 0.5–1.0 mm, all others are 0.25–0.5 mm.

Andes act as a topographic barrier between the humid Amazon Basin and the more arid Pacific margin to the west. Condensation of Atlantic-derived moisture on the eastern Andean flank leads to focused orographic precipitation in the eastern part of the Andean fold-thrust belt with dry conditions on the western plateau region (Lenters and Cook, 1995; Insel et al., 2009).

3. Methods

3.1. Cosmogenic radionuclide data

Modern river sediments were collected from four catchments along a northern transect and thirteen tributaries and trunk streams in a southern transect (Fig. 1a, Table 1). In the northern transect, our CRN samples are mainly from the SA with elevations between 600 and 1400 m, with previous data focused on the high elevation sites (~1600 to 4500 m) in the EC (Figs. 1a, 2a) (Safran et al., 2005). In the southern transect, CRN data are from basins that span a wide range of basin mean elevations from 840 to 3500 m, but again focused in the SA (Table 1). Drainage areas upstream of sample locations vary in size and range from 4 km^2 to 5200 km^2. Samples were collected from within the active channel, focusing on the medium to small sand size fraction.

Samples were washed, dried, and sieved to isolate the grain size fraction between 0.25 and 0.5 mm. In some cases, coarser size fractions between 0.5 and 1.0 mm were used to evaluate the effect of grain size on denudation rate (Table 1). Quartz was separated using standard mineral separation techniques. To eliminate possible contamination by ^{10}Be produced in the atmosphere, quartz was leached with a mixture of hydrofluoric and nitric acid. After dissolution of quartz and

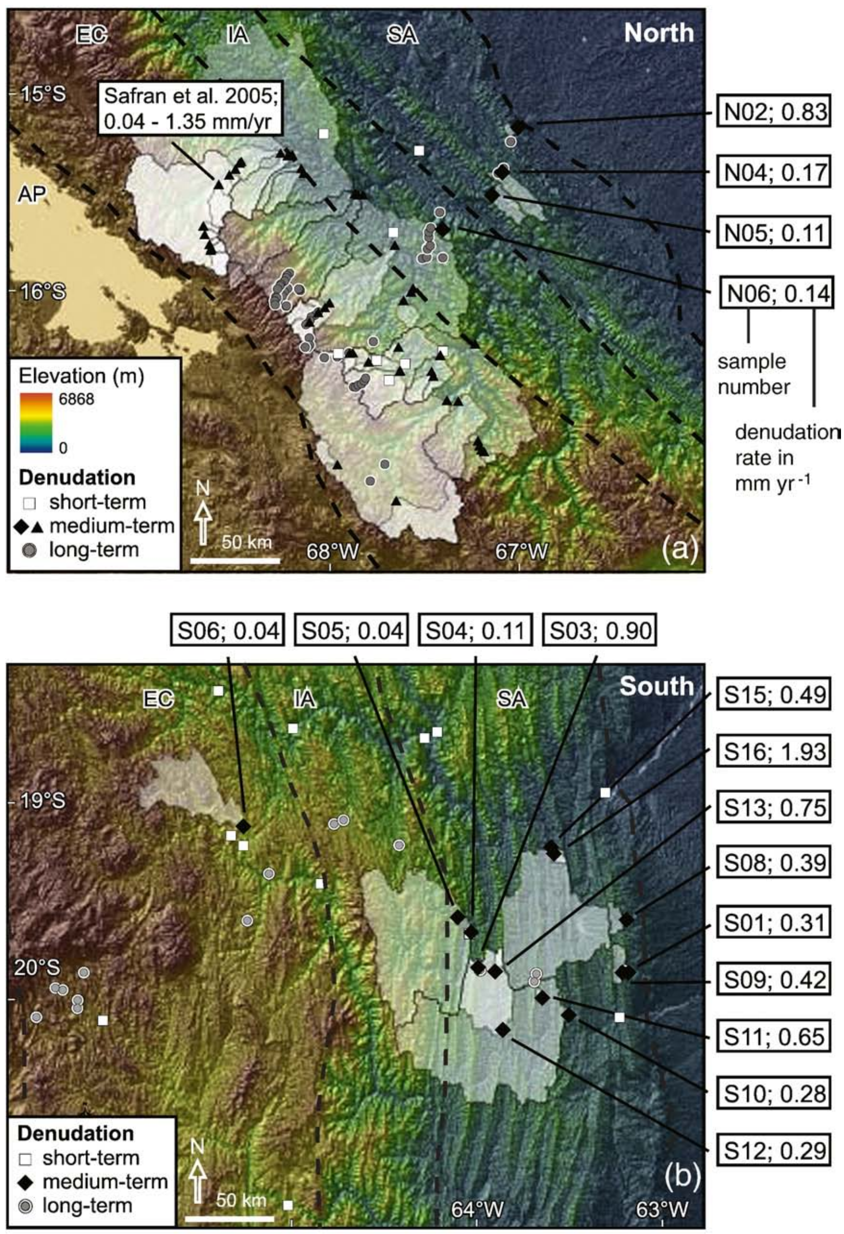

Fig. 2. Thrust belt topography and CRN-derived denudation rates across northern and southern Bolivia in map view (see Suppl. 2 for short and long-term rates). Topography is the 90 m SRTM DEM with basin outlines and sample locations in the northern transect (a) and southern transect (b). Basin sizes sampled vary between 7 and 7000 km^2. Different symbols represent different timescales of denudation: short-term rates (white squares) are gauging station locations (from Barnes and Pelletier, 2006); medium-term represents cosmogenic radionuclide (CRN)-derived denudation rates (in mm yr^{-1}) for the outlined basins in this study (black diamonds) and Safran et al. (2005) (black triangles); and long-term rates (gray circles) represent locations of apatite fission track (AFT) data (from Barnes et al., 2006; Gillis et al., 2006; Safran et al., 2006; Barnes et al., 2008; McQuarrie et al., 2008b). AP: Altiplano, EC: Eastern Cordillera, IA: Interandean zone, SA: Subandes.

addition of ^{9}Be spike, Be and Al were separated by extraction and precipitation following von Blanckenburg et al. (1996). Measurements by accelerator mass spectrometry were carried out at PRIME Lab, Purdue University.

Average production rates for each sample site were calculated using the 90 m SRTM DEM taking into account scaling to latitude and altitude and topographic shielding for each pixel in the DEM (Stone, 2000; Balco, 2001). We used a total production rate of 5.1 atoms g^{-1} yr^{-1} for ^{10}Be and 31.1 atoms g^{-1} yr^{-1} for ^{26}Al at sea level sites and high latitude (Stone, 2000). To account for spallogenic and muonic production, we used spallogenic fractions of 0.978 (^{10}Be) and 0.974 (^{26}Al) contributing to the total production rate (Stone, 2000), while the remaining fraction was assigned to slow and fast muons, using a ratio of 0.53 to 0.47 (Heisinger et al., 2002). The original ICN standard (Nishiizumi et al., 2007) was used as reference standard for measurements and values of 4.62×10^{-7} yr^{-1} (^{10}Be) and 9.68×10^{-7} (^{26}Al) were assigned for the decay constants, respectively. Table 1 lists the production rates for each basin, calculated ^{10}Be and ^{26}Al concentrations, catchment-wide denudation rates, and the corresponding errors after Schaller et al. (2001; 2002).

Ratios of $^{26}Al/^{10}Be$ in our samples are between 3.6 and 6.2. The range of the ratios is consistent with $^{26}Al/^{10}Be$ ratios from Safran et al. (2005), although the average of 4.3 is much lower than the assumed production ratio of 6.1. The catchments with lower ratios were mostly basins with Al content close to the detection limit. We interpret that sediment storage is not responsible for production ratios below 6 (see Discussion section) and assume that the lower ratios are a result of incomplete recovery of stable Al during sample processing (e.g. Safran et al., 2005).

3.2. Long-term denudation rates

Long-term denudation rates were estimated from previously published AFT data (Suppl. 1) (Barnes et al., 2006; Gillis et al., 2006; Safran et al., 2006; Barnes et al., 2008; McQuarrie et al., 2008a). We only account for samples along our two transects and AFT analyses with more than 10 grains per sample. To estimate long-term denudation rates from AFT data, we used the most straightforward method of dividing a presumed closure isotherm depth by the cooling age and assuming a linear, temporally invariant geothermal gradient. For the calculation, we assumed (1) an average AFT closure temperature of 110 °C, (2) average surface temperatures of 10 °C for the EC, 15 °C for the IA, and 23 °C for the SA, and (3) previously estimated values of the geothermal gradient based on proximal borehole-measurements (Barnes et al., 2006, 2008).

The estimated geothermal gradient for the northern transect is 22 ± 2.2 °C/km for the EC, IA, and SA, while in the southern transect we use a gradient of 27 ± 11 °C/km for the EC and the IA, and 18 ± 5 °C/km for the SA. Where available, we estimated long-term denudation rates based on sample cooling histories quantified with inverse thermal modelling (Barnes et al., 2006; Gillis et al., 2006; Barnes et al., 2008). In these cases, instead of using the cooling age, we used the onset of the most recent rapid cooling from the best-fit thermal model to calculate denudation rates (Suppl. 1). We also re-calculated previously estimated long-term denudation rates from Safran et al. (2006) to make them comparable with the data above. With the smaller geothermal gradient re-calculated denudation rates are mostly the same within error as originally reported, with a few exceptions up to 0.3 mm yr^{-1} higher (compare Suppl. 1 and Safran et al. (2006)).

Our calculated denudation rates from thermochronometer samples are only an estimate of true denudation rates over this timescale. Temporal variations in the thermal gradient due to transient denudation, magmatism, and/or removal of overlying units with significantly different thermal conductivity could all introduce uncertainty into these estimates (Ehlers et al., 2005). Addressing these complications often requires detailed thermal modelling of sample cooling histories and various thermo-tectonic processes, an endeavour beyond the scope of this study, and poorly constrained with available data. Rather, we report long-term denudation rates with conservative uncertainties (e.g. Fig. 4) related to the large variability in present-day heat flow in each physiographic unit (after Barnes et al., 2006, 2008). This approach provides an empirically-derived estimate for long-term variations in denudation rates based on known variations in the present-day thermal structure of the Andes.

4. Results

4.1. Spatial variations in CRN-derived denudation rates

Denudation rate estimates based on CRN analyses were calculated from 17 basins (Table 1 and Fig. 2). The rates vary by two orders of magnitude from 0.04 to 1.93 mm yr^{-1} and indicate apparent ages of 0.4 to 20 ka. More than 75% of the basins have an apparent age younger than 5 ka.

In the northern transect, three samples from the northern SA and one from the IA were measured (Figs. 2a, 3a). The denudation rates vary by a factor of 8 and range from 0.11 to 0.83 mm yr^{-1} over apparent ages of 1.0 to 7.1 ka (Table 1). The highest denudation rate observed (0.83 mm yr^{-1}) is in a small basin (N02) located along the frontal range of the SA (Figs. 2a, 3a). To the west, denudation rates are smaller with magnitudes ~0.1–0.2 mm yr^{-1} (Figs. 2a, 3a). Denudation rates are similar for the SA and the IA. Because samples were only available from four basins, general trends in the denudation rates are difficult to define robustly. However, the range of denudation rates is in good agreement with CRN-derived denudation rates for basins in the EC that range between 0.04–1.34 mm yr^{-1} (Figs. 2a, 3a) (Safran et al., 2005). The mean value for all calculated CRN-derived denudation rates in the northern transect is 0.40 ± 0.29 mm yr^{-1}, including published rates by Safran et al. (2005). Denudation rates for different grain sizes of the same sample do not show noteworthy differences (Table 1).

In the southern transect, 11 samples from the southern SA, 1 from the IA, and 1 from the EC were measured (Figs. 2b, 3b). The denudation rates vary by two orders of magnitude from 0.04 to 1.93 mm yr^{-1} with apparent ages of 0.4 to 20.3 ka (Figs. 2b, 3b, Table 1). Most sampled basins are located entirely within the SA. One SA basin (S16) indicates an exceptionally high denudation rate of 1.93 mm/yr. Although the sample appears as an outlier relative to the other samples we include it in our analysis because there were no anomalous aspects of the drainage basin (e.g. recent large landslides) or abnormalities in the chemical analysis that would preclude consideration. A denudation rate of 0.1 mm yr^{-1} is calculated for a basin (S04) situated mainly in the IA. The one EC basin (S06) indicates one of the lowest denudation rates with a magnitude of 0.04 mm yr^{-1}. The mean CRN-derived denudation rate for the south is 0.51 ± 0.50 mm yr^{-1}.

4.2. Temporal variations in denudation rates

Transients in the denudation rates are observable when comparing rates calculated over long- (AFT-derived), medium- (CRN-derived) and short-timescales (sediment flux-derived) (Fig. 4). Results shown compare our CRN-derived rates with long-term rates calculated from published AFT data (see Section 3.2) and short-term rates from sediment gauging stations neighboring our sample locations. Sediment flux determinations include the total suspended and dissolved loads and are thought to be representative of the modern physical denudation rates (Barnes and Pelletier, 2006; see also Aalto et al., 2006).

In the northern transect, short-term denudation rates were calculated from 9 sediment gauging stations that recorded sediment fluxes from drainage basins ranging in size from 270 to 67,200 km^2

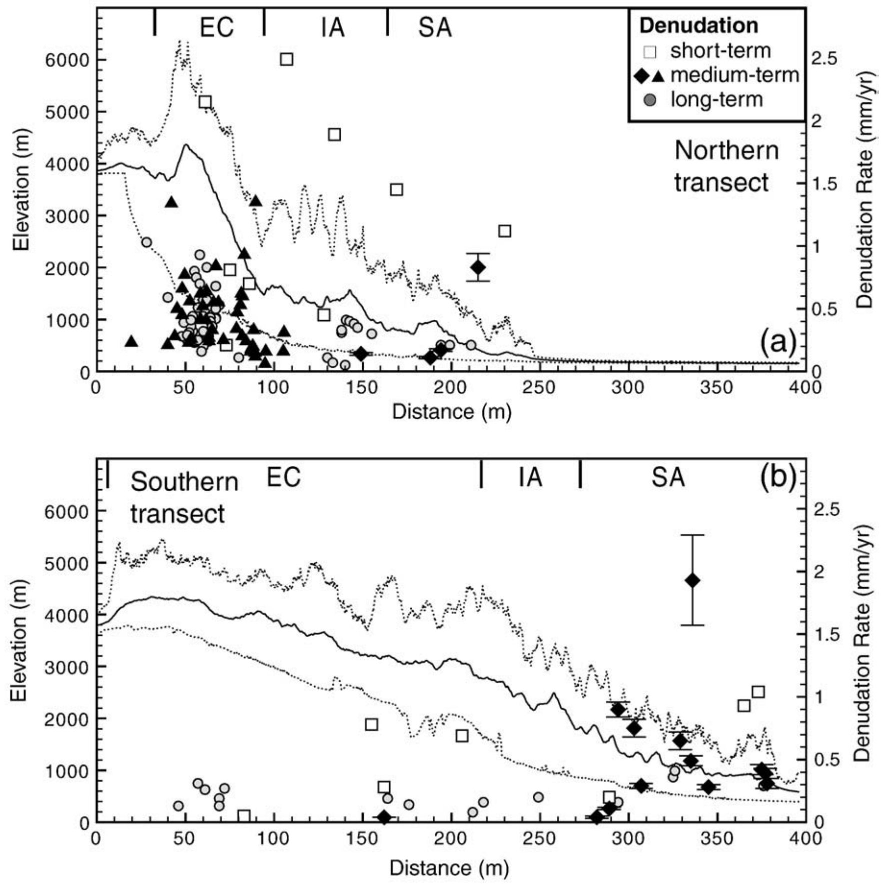

Fig. 3. Variations in topography and denudation along the northern (a) and southern (b) transects in cross-section (see Fig. 1 for locations). The 200 km-wide swath topography profiles of maximum, minimum (dashed grey lines) and mean altitudes (solid black lines) are based on the 90 m SRTM DEM and are oriented perpendicular to the fold-thrust belt. EC: Eastern Cordillera, IA: Interandean zone, SA: Subandes. Long-, medium-, and short-term denudation rates are plotted along the profiles.

(Figs. 2a, 3a) (Guyot et al., 1988; Barnes and Pelletier, 2006). Short-term denudation magnitudes vary between 0.21 and 2.49 mm yr^{-1}, with a mean denudation rate of 1.25 ± 0.79 mm yr^{-1} and are therefore two to three times higher than medium-term denudation rates (mean of 0.40 ± 0.29 mm yr^{-1}, Fig. 3a, 4). AFT data from the northern transect indicate long-term denudation rates of ~0.1–1.0 mm yr^{-1} (mean of $\sim 0.42 \pm 0.19$ mm yr^{-1}) for the EC, 0.05–0.4 mm yr^{-1} (mean of $\sim 0.27 \pm 0.15$ mm yr^{-1}) for the IA and 0.1–0.2 mm yr^{-1} (mean of $\sim 0.18 \pm 0.06$ mm yr^{-1}) for the SA (Suppl. 1), suggesting a decrease in long-term denudation from southwest to northeast (Fig. 3a). The mean denudation rate based on the AFT data for the entire transect is 0.38 ± 0.19 mm yr^{-1} and is within error similar to the CRN-derived denudation rates (Fig. 4).

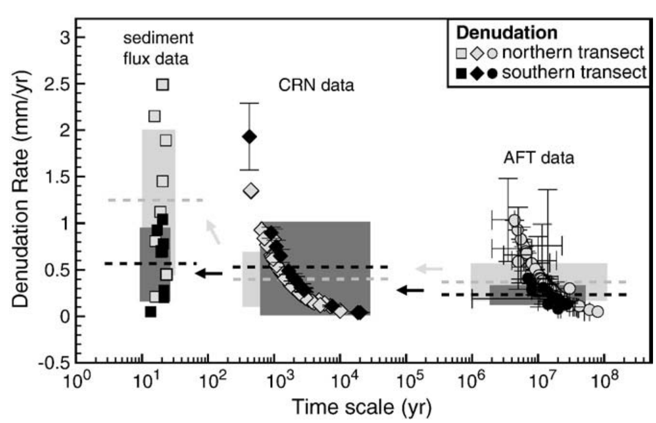

Fig. 4. Comparison of the temporal variations in denudation rates for the northern (light gray) and southern (black) transects in Bolivia. Dashed lines indicate best estimation of mean denudation rates. Solid boxes show one sigma standard deviation of denudation rates. Arrows highlight the change in denudation over time. Circles represent values from apatite fission track data (calculated from previously published data: Barnes et al., 2006; Gillis et al., 2006; Safran et al., 2006; Barnes et al., 2008; McQuarrie et al., 2008b) with error bars representing range of acceptable rates, diamonds show cosmogenic radionuclide-derived denudation rates (this study and from Safran et al., 2005), squares show denudation rates from sediment flux data (Barnes and Pelletier, 2006).

In the southern transect, short-term denudation rates were estimated from 7 gauging stations for drainage basin sizes between 1600 and 59,800 km^2 (Figs. 2b, 3b) (Guyot et al., 1990; Barnes and Pelletier, 2006). Short-term denudation rates range between 0.05 mm yr^{-1} and 1.04 mm yr^{-1}, with a mean value of 0.57 ± 0.39 mm yr^{-1} (Fig. 4). The range and mean of short-term denudation rates in the southern transect are very similar to the medium-term denudation rates (0.51 ± 0.50 mm yr^{-1}, Fig. 4). Long-term denudation rates from AFT data range between ~0.1–0.3 mm yr^{-1} (mean of $\sim 0.20 \pm 0.07$ mm yr^{-1}) for the EC, 0.08–0.2 mm yr^{-1} (mean of $\sim 0.15 \pm 0.06$ mm yr^{-1}) for the IA, and 0.2–0.4 mm yr^{-1} (mean of $\sim 0.31 \pm 0.11$ mm yr^{-1}) or more for the SA (Figs. 3b, 4). The total long-term mean denudation rate estimated from best-fit denudation rates for the southern transect is 0.22 ± 0.09 mm yr^{-1}, indicating that long-term denudation rates in the south are similar to medium-term denudation rates within error (Fig. 4). However, a direct comparison between medium- and long-term denudation rates along the same structures in the southern SA shows a moderate increase in denudation towards the present at specific locations (e.g. S03/SA2, S11/SA3, Suppl. 2).

Caution should be used when comparing short- and medium-term denudation rates from Bolivia due to the limited amount of data available and the large difference in drainage basin sizes used for short timescale sediment flux determinations relative to the CRN-derived rates. For example, although the mean denudation rate in the southern transect is very similar for short- and medium-term timescales, a comparison between individual sites (e.g., S04/PZ, S06/NU, S10/SA) reveals a two to three times higher denudation rate from sediment-flux data than for CRN-derived data (Suppl. 2). This discrepancy in denudation rates may indeed be true for all drainage basins in this region (e.g. if the area is in topographic steady state) but a larger data set is needed from future work to verify this. Differences between short- and medium-scale denudation rates are often associated with humans acting as geomorphic agents (e.g. Hooke, 2000; Wilkinson and McElroy, 2007). However, human population in the Bolivian Andes is relatively sparse and smaller villages in most mountain drainages in the Andes have been populated for millennia (Harden, 2006) with small-scale agricultural practices commencing ~3.5–3.0 ka (e.g. Binford et al., 1997; Paduano et al., 2003). Most of the catchments sampled in this study were selected because they have a very low population density, minimal agricultural activity, and limited to no deforestation and therefore suggest anthropogenic effects on CRN-derived and modern denudation rates are low.

4.3. Denudation rates, morphology and climate

Previous studies have suggested that morphologic parameters (e.g. elevation, relief, slope, lithology, drainage size) and climate-related factors (e.g. precipitation, vegetation, runoff) can have a large influence on denudation rates (e.g. Ahnert, 1970; Pinet and Souriau, 1988; Summerfield and Hulton, 1994; Pazzaglia and Brandon, 2001; Reiners et al., 2003). In this section, we explore the relationships between basin size, mean local relief, slope and elevation, mean annual precipitation, and our CRN-derived denudation rates. Comparison between morphologic and climate parameters is also conducted to investigate if the parameters are the source of the large variability detected in CRN-derived denudation rates.

Previous studies have demonstrated a negative correlation between drainage basin size and denudation that has been suggested to result from the decreasing ratio of sediment production and sediment storage (Summerfield and Hulton, 1994; Hovius, 1998). Fig. 5 shows denudation rate versus sample upstream drainage basin area. Results indicate that denudation rates do not correlate with catchment sizes (r^2<0.11). Drainage areas upstream of CRN sample locations vary largely in size and range from 4 to 10,900 km^2. High medium-term denudation rates with magnitudes exceeding 1 mm yr^{-1} and low medium-term denudation rates with values less than 0.1 mm yr^{-1} are reported for individual basins that differ in size by two orders of magnitude (Fig. 5). Short-term denudation rates are above 1.0 mm yr^{-1} for several basins with areas between 272 and 67,200 km^2 and less than 0.1 mm yr^{-1} for a basin with

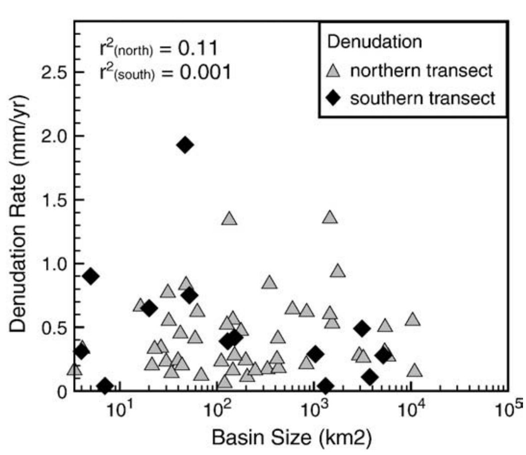

Fig. 5. Cosmogenic radionuclide-derived denudation rates for different basin sizes. The northern transect includes 43 samples from Safran et al. (2005).

4200 km^2 in size. These results show that denudation rates for different basins do not depend on the size of the catchment, and that there is no systematic bias in our comparison of denudation rates from basins of different size. We also find no covariance in denudation rate with basin area and other parameters (e.g. slope or relief), and illustrate this by indicating the drainage basin size in other plots (Fig. 6).

We also find no statistically significant correlation between denudation rates (CRN-derived) and local relief or slope as previously suggested (Fig. 6) (e.g Ahnert, 1970; Pinet and Souriau, 1988; Summerfield and Hulton, 1994; Pazzaglia and Brandon, 2001; Schaller et al., 2001; Montgomery and Brandon, 2002). Northern transect samples including samples from Safran et al. (2005) are mostly from the high-relief region of the EC, while most of the samples from the southern transect are located in the lower-relief SA. However, both transects include samples from all the different thrust belt zones including the EC, IA, and SA and span an overall 2 km-radius relief range from 414 to 1340 m (Table 1). Our data indicate that CRN-derived denudation rates do not correlate with relief (r^2<0.11, Fig. 6a). Denudation rates are between 0.04 and 1.93 mm yr^{-1} for samples with low relief (<750 m) and between 0.04 and 1.35 mm yr^{-1} for samples with higher relief. Slopes are steepest in the northern EC with values up to ~56%, while the mean slope along the southern thrust belt is ~25–30%. Our data do not show a correlation between CRN-derived denudation rates and mean basin slope (r^2<0.05, Fig. 6b). In addition, no correlation exists between CRN-derived denudation rates and sample elevation (r^2<0.28, Fig. 6c). However, a moderate correlation exists between CRN-derived denudation rates and elevation, relief, and slope respectively for big basins with a drainage area >1000 km^2 in the southern transect with r^2 values between 0.7 and 0.8.

The impact of modern climate, and in particular precipitation, on denudation rates is still debated (e.g. Riebe et al., 2001; Burbank et al., 2003; Reiners et al., 2003). As described above, latitudinal variations in orogen width, exhumation depth, and rock uplift rate in the central Andes have been attributed to a long-strike differences in climate and associated denudation. Fig. 7 shows the range of short- and medium-term denudation and precipitation rates for the northern and southern transects. The present-day climate pattern is based on an interpolation of a network of rainfall stations (Peterson and Vose, 1997). This approach has the benefit of providing calculated climate norms over a longer times scale (10 to ~90 yr), but has the shortcoming of missing local orographic variations in climate between stations. To address the potential variability in local climate missed in the stations we compared our precipitation rates over each drainage basin to a shorter term (~8 yr) and higher spatial resolution record determined from TRMM satellite data (Bookhagen and Strecker, 2008). In general, we find that the historical climate data capture regional spatial variations in the mean precipitation rate, and have the added advantage of providing a climate norm calculated over multiple El Niño cycles (e.g. Fig. 1b).

Short-term sediment flux-derived denudation rates are consistent with the modern precipitation pattern but medium-term CRN-derived rates are not. The northern transect increases in precipitation from ~500 mm yr^{-1} in the southwest to ~1700 mm yr^{-1} in the northeast (Figs. 1b, 7a). The southern transect is characterized by low precipitation from between 250 mm yr^{-1} in the west to ~700 mm yr^{-1} in the east (Figs. 1b, 7b). The sediment flux-derived mean denudation rate is 2–3 times higher in the northern transect than in the southern transect, reflecting the precipitation gradient with decreasing rates from the north to the south (Fig. 7). However, CRN-derived mean denudation rates in the north and south are essentially the same within 1σ error (0.40 ± 0.29 mm yr^{-1} vs. 0.51 ± 0.50 mm yr^{-1}), indicating that denudation rates averaged over several thousand years do not correlate with the present-day latitudinal climate gradient (Fig. 7). Moreover, basins in the northern SA, where precipitation is highest, show the same range in CRN-derived denudation magnitudes as previously estimated rates for

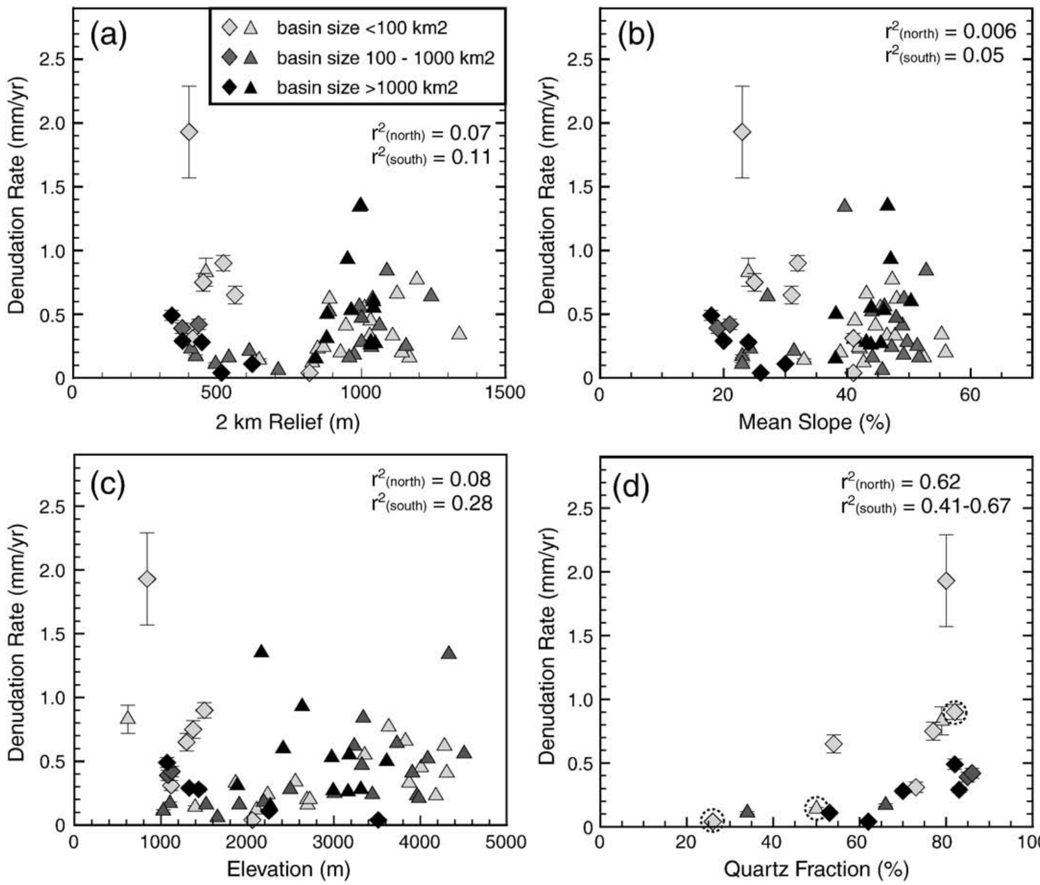

Fig. 6. Cosmogenic radionuclide (CRN)-derived denudation rates versus geomorphologic indices resolved for basin sizes. Diamonds represent samples from the southern transect, triangles are denudation rates from the northern transect. The northern transect includes 43 denudation rates from Safran et al. (2005). (a) CRN-derived denudation rates versus relief (2 km radius). No statistical correlation exists. (b) CRN-derived denudation rates versus mean basin slope. No statistical correlation can be detected. (c) CRN-derived denudation rates versus elevation. No statistical correlation exists. (d) CRN-derived denudation rates versus quartz content. Weak positive correlation. Quartz yield represents rate of weathering, not an index for lithology. Dotted circles mark the three Devonian samples to highlight the discrepancy between quartz content and lithological age.

the more arid EC (Fig. 7a) (Safran et al., 2005). In the southern transect, differences in mean annual precipitation between individual sample locations along the profile are too small to determine a correlation between climate and denudation.

The precipitation in the Bolivian Andes is highly seasonal with ~80% of precipitation falling in austral summer (Garreaud, 2000). Previous studies have suggested that denudation is related to storm activity and extreme precipitation events rather than mean annual precipitation (e.g. Coppus and Imeson, 2002). We have compared denudation rates with maximum summer precipitation, in addition to the mean annual rainfall reported above, and come to the same conclusion; no direct relationship can be found between CRN-derived denudation rates and summer precipitation.

5. Discussion

Previous studies suggest several factors influence spatial and temporal variations in orogen denudation. For example, Montgomery and Brandon (2002) showed a linear relationship between denudation magnitude and mean slope for tectonically inactive regions with a mean slope <25º and either a weak linear or strong non-linear relation between denudation rate and mean slopes >30º in active tectonic settings. A correlation between climate and denudation has been found locally in areas where precipitation varies by an order of magnitude (Reiners et al., 2003). Alternatively, settings where large temporal variations in climate influence hillslope processes and vegetation (Schaller et al., 2002) have led to the interpretation that pronounced climate change might exert a larger control over denudation than the inter-regional climate variability (von Blanckenburg, 2005). Recent work by Stock et al. (2009) in the tectonically active and partially glaciated Wasatch Mountains, Utah, USA has documented large spatial and temporal variations in denudation recorded from similar geo- and thermochronology approaches as used in this study. Results from the Wasatch Mountains and the Bolivian Andes, including those presented here, do not show clear relationships between denudation, tectonics, climate, or landscape morphology thereby making it difficult to determine the factors influencing denudation rates. In the following, we discuss possible reasons for the observed spatial and temporal variations in denudation.

5.1. Lithologic and tectonic controls on denudation rates

The large range in calculated denudation rates (Table 1, Fig. 2) could be the result of local basin characteristics. For example, differences in lithology and the erodibility of different rock types have been suggested as a noticeable effect upon denudation rates in the Bolivian Andes (e.g. Aalto et al., 2006). Previous studies have classified the lithologies in the region into a small number of homogenous groups (igneous, meta-sedimentary, weak-sedimentary rocks) and ascribed an index representing the quartz content or the relative rates of chemical erosion to account for different rock strength (Safran et al., 2005; Aalto et al., 2006). Safran et al. (2005) corrected their CRN-derived denudation for the quartz content in different lithologies by ascribing a higher quartz fraction to areas underlain by plutons, conglomerates, and late Miocene deposits. The

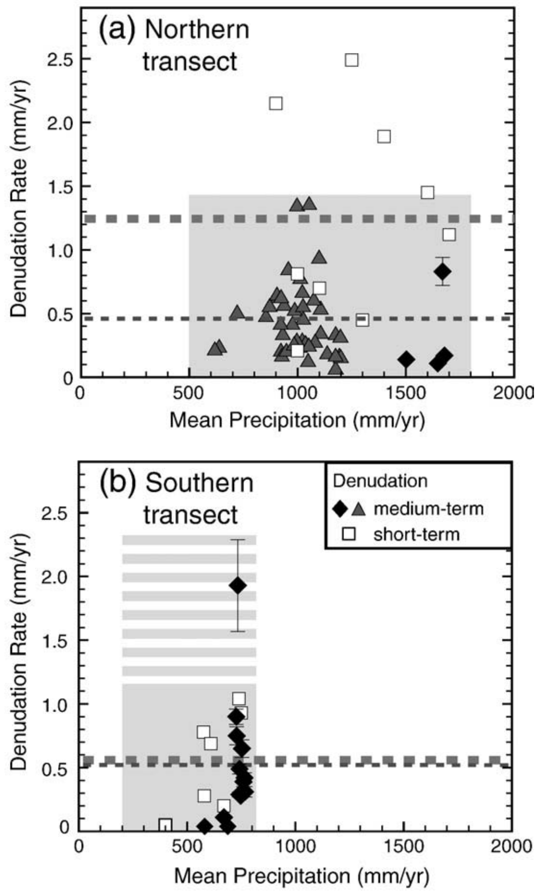

Fig. 7. Latitudinal variations in denudation and precipitation across two transects in Bolivia. Medium-term (CRN-derived) denudation rates in the north include samples from Safran et al. (2005) (grey triangles, diamonds are from this study). Short-term (sediment flux-derived) denudation rates are from Barnes and Pelletier (2006) (white squares). The gray box highlights the range of medium-term denudation (striped part includes the exceptionally high rate) and precipitation. The thin dashed line represents mean medium-term denudation rates (calculated for all samples in each transect), the thick dashed line represents mean short-term denudation rate. (a) Northern transect. (b) Southern transect.

correction for local quartz fraction made a relatively small difference to the overall frequency distribution of denudation rates. In most of the basins characterized by a >20% difference between corrected and uncorrected estimated denudation rates the quartz-rich lithologies (i.e. plutons) occupy high terrain and the correction resulted in an increase in estimated denudation. Lithologies within our sampled catchments are composed of metasedimentary rocks and all fall into the same previously defined groups of erosive indexes, despite their differences in stratigraphic age (Table 1). Therefore, we assume that the underlying lithology in the study area does not have a direct effect on denudation rates. However, we estimated the quartz yield for each sample based on the quartz content derived from the sample material (e.g. the amount of quartz in relation to other minerals within the sample). The quartz yield in the analyzed grain size fraction for individual samples spans a wide range between 34% and 83%. These percentages do not reflect the quartz distribution in the source lithologies, but instead most likely indicate the degree of weathering for different sample sites. For example, small basins exposing Devonian aged metasediments have a large variance in quartz contents of 26, 50, and 82% (Table 1, Fig. 6d). Catchments with the lowest denudation rates show low quartz content, while catchments with high denudation rates are characterized by material with high abundance of quartz (Fig. 6d).

High denudation rates found in some of the smaller basins (e.g. N02, S03, S11, S13, S16) may reflect active faulting along basin bounding thrusts, but in general, we find no relationship between denudation rates and structural activity of different regions. What is known is the SA are the most tectonically active part of the central Andean fold-thrust belt and characterized by broad, large wavelength synclinal basins separated by narrow zones of thrust-faulted anticlines (e.g. Baby et al., 1992; Dunn et al., 1995; Lamb, 2000). Evidence for recent deformation along previously mapped faults is not present. For example, field mapping and analysis of aerial photos at each sample location does not show recent faulting or landsliding in the sampled catchments. In addition, modern earthquakes in the region are typically moderate to deep in depth (~20 to 30 km in the north, between 50 and 600 km in the south) and associated with deeper subduction related deformation rather than near surface Holocene to Quaternary deformation (IRIS, 2009).

We might expect erosion rates to reflect the dominantly eastward propagation of SA deformation with time. Unfortunately, evidence for out-of-sequence deformation exists (e.g. Barke and Lamb, 2006; Uba et al., 2009) but is poorly constrained relative to the temporal scales over which the CRN-derived denudation rates average. Some basins (e.g. N02) are located along the frontal range and have high denudation rates perhaps reflective of active deformation whereas others (N04, N06) are located within major thrust faults but exhibit low denudation rates, possibly due to locally reduced deformation. In the southern transect, small basins with high denudation rates (e.g. S03, S11, S13, S16: >0.65 mm yr^{-1}) lie in the hanging walls of major thrust faults in the western part of the SA, while basins located along the frontal range (e.g. S01, S08, S09) have intermediate denudation rates of ~0.3 to 0.4 mm/yr. This pattern could be recent out-of-sequence deformation that would result in the frontal-most structure not being the most active one (e.g. Barke and Lamb, 2006; Uba et al., 2009). However, other calculated denudation rates do not correlate with tectonic structures in the SA. For example, basin S05 has the lowest denudation rate (0.04 mm/yr) despite the high relief, steep slopes and a location within the hanging wall of a major thrust fault. In summary, no obvious relationship exists between CRN-derived denudation rates and fault activity.

5.2. Sediment transport and storage

One of the most prominent processes that might influence spatial and temporal variations in catchment denudation is mass-movements such as landslides. Landslides are an important source of sediment supply that might lead to overestimation of denudation rates derived from CRN data (e.g. Hovius et al., 2000; Gabet et al., 2004). Alternatively, modeling studies have shown that in some landslide dominated landscapes CRN-derived denudation rates can underestimate the true catchment-averaged denudation rate in small catchments (Niemi et al., 2005; Yanites et al., 2009). However, our sampled regions are not landslide dominated, and it is unlikely that the small basin S05 (~7 km^2) that is characterized by very low denudation (0.04 mm yr^{-1}, Fig. 2) but high relief (~820 m) and steep slopes (40%) can be attributed to an underestimation of denudation due to landsliding. Nevertheless, landslides are prominent features in the northern EC (e.g. Blodgett and Isacks, 2007) and we suggest that the variability in medium- and short-term denudation in these basins could be in part ascribed to mass-wasting processes.

Temporal storage of sediment within drainage basins could influence CRN abundance and therefore medium-term denudation rates (Bierman and Steig, 1996). Sediment storage within a catchment can increase the measured CRN concentration if sediments are exposed, or alternatively decrease the concentration if sediments are shielded by burial and CRN decay. More sediment storage would be expected in larger basins, but none of the big rivers in the study area show extensive floodplains within the Andes, and instead generally cut through the steep, high relief terrain. A relatively short and fast sediment cycle has been observed for large basins (~10^3 and 10^6 km^2 drainage area) in the northern Bolivian Andes with a residence time for sediments of only ~3 ka (Dosseto et al., 2006). In this study, we sampled significantly smaller catchments with lower residence times and CRN-derived denudation rates incorporating several sediment cycles. No additional CRN accumulation is observed during sediment storage so the cosmogenic denudation signal is preserved (Wittman et al., 2009; Wittmann and Blanckenburg, 2009).

The short-term denudation rates derived from sediment-flux data could be potentially biased by modern sediment cycle conditions. Sediment transport and deposition are highly dynamic processes that vary over time and short-term denudation rates from sediment flux data are subject to seasonal-to-decadal-scale fluctuations and the effects of transient sediment storage (e.g. Kirchner et al., 2001). Therefore, short-term denudation rates might reflect only a specific episode within the transport cycle that records a phase of high sediment flux or high sediment storage on decadal timescales. For example, a detailed study of the Pilcomayo River in southern Bolivia revealed interannual variability in river discharge related to El Niño/Southern Oscillation (ENSO) with lower discharge during El Niño Years (Smolders et al., 2002).

5.3. Potential influence of Holocene climate change on denudation

Holocene climate and vegetation change could be an explanation for the observed temporal differences in denudation rates and the discrepancy between medium-term denudation and present-day precipitation. Terrestrial paleoclimate records indicate significant climate variations on millennial and orbital timescales affected the central Andes (Baker et al., 2001a; 2001b; Abbott et al., 2003). Major changes in lake levels, lake sedimentation (Cross et al., 2000; Rowe et al., 2002; Abbott et al., 2003), and vegetation (Graf, 1981; Bush et al., 2005) suggest changes in both precipitation and temperature. Central Andean paleoclimate records show an overall pattern of aridity from the late Pleistocene through the MH in Bolivia (e.g. Cross et al., 2000; Baker et al., 2001b; Rowe et al., 2002; Abbott et al., 2003; Servant and Servant-Vildary, 2003).

Climate changes in the central Andes were linked to modifications in insolation due to changes in orbital parameters, ENSO, and Atlantic sea surface temperatures (e.g. Baker et al., 2001a,b; Moy et al., 2002; Servant and Servant-Vildary, 2003). ENSO is the most likely reason for precipitation changes on MH timescales and is driven by orbital fluctuations. ENSO is an important factor in the modern climate system over the Andean region with a weak tendency towards below average precipitation during El Niño summers over the Bolivian Altiplano (Vuille, 1999). Model results and observations have shown significant variations in the strength and frequency of ENSO in the past with (1) a more El Nino-like climate stage between 8 and 5 ka (Rollins et al., 1986; Sandweiss et al., 1996), (2) a steady increase in warm ENSO events over the Holocene, with a peak intensity and frequency of these events at ~1.2 ka (Clement et al., 2000; Moy et al., 2002), and (3) a larger ENSO variability in the last 1.5 ka (Moy et al., 2002; Servant and Servant-Vildary, 2003).

The effects of ENSO variability are different in the northern and southern regions of Bolivia. In the northern Bolivian Andes, the MH dry phase (~6 ka) was followed by large magnitude climatic change including a sharp increase in stormy type precipitation between 4.5 and 3.2 ka and an intensification of erosion in the Lake Titicaca watershed on the Altiplano between 4.5 and 2.7 ka (e.g. Abbott et al., 1997; Servant and Servant-Vildary, 2003). After 2.7 ka, coinciding with an increased frequency in El Niño, Lake Titicaca decreased and erosion weakened in the north of the Bolivian Andes, while precipitation was more uniformly distributed (Servant and Servant-Vildary, 2003). These conditions persisted until 0.5 ka, coinciding with the highest El Niño variability of the Holocene. However, convective

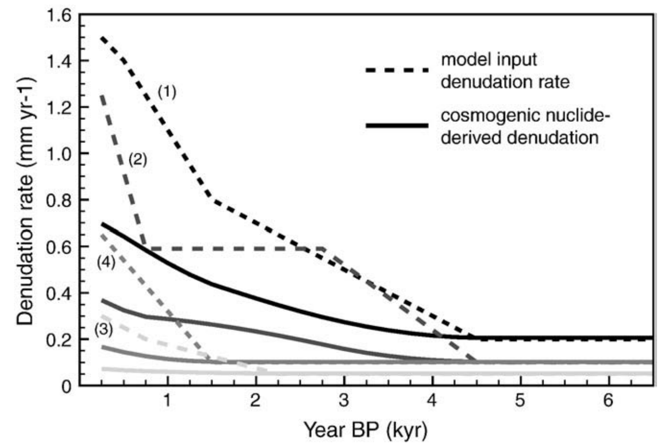

Fig. 8. Model calculation of the sensitivity of cosmogenic radionuclide-derived denudation rates to changing climate conditions between the mid-Holocene and the present (e.g. Baker et al., 2001b; Abbott et al., 2003; Servant and Servant-Vildary, 2003). Four different scenarios are presented: (1) a steady increase in denudation rate since 4.5 ka with an input denudation rate for the arid period before 4.5 ka of 0.20 mm yr^{-1}, a constant increase in denudation to 0.80 mm yr^{-1} at 1.5 ka and a steeper increase in denudation to 1.5 mm yr^{-1} at present times (black dotted line); (2) an initial denudation rate of 0.10 mm yr^{-1} with an increase to 0.59 mm yr^{-1} between 4.5 and 2.75 ka, a period of constant denudation until 0.75 ka and a significant increase to 1.25 mm yr^{-1} at modern times (dark gray line); and (3 and 4) calculated cosmogenic nuclide denudation histories for an increase in denudation rate since 2.25 ka and 1.5 ka, respectively, with initial denudation rates of 0.05 and 0.10 mm yr^{-1} and a steady increase to 0.3 and 0.7 mm yr^{-1} at present (medium and light gray lines).

rainfall did not reach the southern Bolivian Andes and dry conditions remain as evident from aeolian sand dunes, dated 3.5 to 2 ka, extending along the Andes between 18° and 23°S (Servant et al., 1981). The onset of modern conditions in the southern part of the Bolivian Andes was much later than in the north and took place at ~2.3 ka (e.g. Abbott et al., 2003).

Significant differences between present-day precipitation patterns and climate conditions during the past could have an intrinsic effect on denudation in the central Andes. Denudation rates averaged over thousands of years would not reflect the distinct climate characteristics of today, but would (at least partially) possess an inherited signal from the previous climate. We quantify the potential effect of climate change on CRN-derived denudation rates (Fig. 8). A numerical model was used to evaluate the sensitivity of CRN-derived denudation rates to temporal variations in climate and denudation (for model details see Schaller et al., 2002; Schaller and Ehlers, 2006). The model uses a climate-driven input denudation history to calculate a cosmogenic ^{10}Be-derived denudation history (Schaller et al., 2001). Temporal variations in the surface and subsurface CRN concentrations for each time step are calculated by numerical integration of a depth-dependent production based on the input denudation rate from the previous step. In our simulations for the Bolivian Andes, we assume low denudation (0.05–0.2 mm yr^{-1}) rates during the MH due to the recorded aridity in Bolivia for our initial conditions. Next, we invoke an increase in denudation rates to modern values (0.30–1.5 mm yr^{-1}) in different time-step scenarios reflecting an onset of wetter conditions (Cross et al., 2000; Abbott et al., 2003). The magnitude of increase in denudation rates associated with wetter conditions in the Andes is unknown. Given this, a plausible range of increases in denudation is explored by evaluating four difference scenarios for the magnitude of denudation rate changes between 0–4.5 ka.

The model settings reflect continuous increase in denudation since 4.5 ka and 2.25 ka respectively, imitating the onset of wetter conditions in the northern and southern part of the Altiplano (Fig. 8, (1) and (3)). A stepwise increase in denudation since 4.5 ka, with higher denudation between 4.5 to 2.7 ka, a constant denudation until 0.5 ka, and modern increase in denudation reflects the observed precipitation and denudation pattern in the northern Andes (Fig. 8, (2)). A uniform increase in denudation for the last 1.5 ka is related to the high ENSO variability during that time interval (Fig. 8, (4)). Calculated modern CRN-derived denudation rates at the end of each simulation vary between 0.07 and 0.7 mm yr^{-1} and are in good agreement with our observations. The simulations indicate that changes in precipitation lead to a slow adjustment of the CRN concentration, but that it can take thousands of years before the CRNs are in complete equilibrium with the new climate (or denudation) conditions as previously noted (Schaller et al., 2001; Niemi et al., 2005; Schaller and Ehlers, 2006). This conclusion is consistent with a recent study that ascribed fluctuations between high and low denudation periods to changes in climate over medium-term timescales (Dosseto et al., 2006).

In summary, the 3-fold discrepancy between short- and medium-term denudation rates in northern Bolivia can be reconciled if the following conditions are met: (a) aridity in the MH causing very low (<0.1 mm yr^{-1}) denudation rates, (b) an onset of wetter conditions between 4.5 and 1.5 ka was accompanied by increasing denudation rates, and (c) overall changes in denudation rates are large over medium-term timescales.

6. Implications and conclusions

Our results exhibit large spatial and temporal variations in denudation rates across the central Andes in Bolivia. Cosmogenic ^{10}Be concentrations from modern river sediments indicate catchment-averaged denudation rates of 0.04–1.93 mm yr^{-1} with apparent ages of 0.4 to 20 ka. No statistically significant correlation exists between CRN-derived denudation rates and morphological indices such as relief, slope or basin size. However, smaller basins reflect a much higher variability in denudation rates, probably due to local basin parameters (e.g. proximity to active faults,). Latitudinal variations in precipitation are not reflected in the CRN-derived denudation rates.

Denudation rates averaged over long- (>10^6 yrs) and medium-term (10^2–10^4 yrs) timescales are similar and within error of each other. Consistency between CRN-derived denudation rates and the much longer-term fission-track exhumation rates implies that on average denudation rates over the last several millions years in the central Andes might have been similar. However, a comparison between best-fit denudation rates estimated from AFT data and CRN-derived data from similar locations along the southern transect suggest at the 1σ-level a moderate increase in denudation rates over time. The along-strike contrast in denudation might have existed since the Miocene, but the total magnitude is difficult to constrain due to large errors associated with the long-term denudation magnitudes.

A significant increase in denudation rates over the last several thousand years is observed with sediment flux-derived denudation rates ~3 times higher than CRN-derived denudation rates in the northern transect. Our data, which cover a previously sparsely sampled medium-term timescale, indicate that the increase in short-term (10^1 yrs) denudation rates is relatively recent and that it might be associated with an increase in precipitation since ~4.5 ka. Climate model simulations of the study area indicate that the Bolivian Andes likely experienced a general increase in precipitation since the mid-Holocene. Climate shifts towards more humid conditions and/or towards more variable conditions in the Bolivian Andes may have had a substantial influence on denudation rates.

In summary, our results suggest that the effect of an increase in Holocene precipitation rates over the last ~4.5 ka on denudation rates is prevalent in the CRN data. Thus, CRN data from the central Andes may not reflect the modern climate. Other factors that might have contributed to the recent increase in denudation rates are an increase in sediment yield and/or the sensitivity of sediment flux data to episodic changes in denudation or storage that may influence such data over short time scales.

Acknowledgements

We thank SERGIOTECMIN of La Paz, Bolivia, and Jaime Tito for logistical support. Financial support was provided to T. Ehlers and C. Poulsen by the US National Science Foundation (EAR 0738822 and 0544954), two University of Michigan Scott Turner Awards in Earth Sciences to N. Insel, and a University of Michigan Sokol International Summer Research Fellowship in the Sciences to J. Barnes. We thank two anonymous reviewers for their insightful comments that greatly improved the manuscript.

Appendix A. Supplementary material

Supplementary data associated with this article can be found, in the online version, at doi:10.1016/j.geomorph.2010.05.014.

References

Aalto, R., Dunne, T., Guyot, J.L., 2006. Geomorphic controls on Andean denudation rates. Journal of Geology 114, 85–99.
Abbott, M.B., Binford, M.W., Brenner, M., Kelts, K.R., 1997. A 3500 14C yr high-resolution record of water-level changes in Lake Titicaca, Bolivia/Peru. Quaternary Research 47, 169–180.
Abbott, M.B., Wolfe, B.B., Wolfe, A.P., Seltzer, G.O., Aravena, R., Mark, B.G., Polissar, P.J., Rodbell, D.T., Rowe, H.D., Vuille, M., 2003. Holocene paleohydrology and glacial history of the central Andes using multiproxy lake sediment studies. Palaeogeography, Palaeoclimatology, Palaeoecology 194, 123–138.
Aceituno, P., 1988. On the functioning of the southern oscillation in the South American sector. Part I: Surface climate. Monthly Weather Review 116, 505–524.
Ahnert, F., 1970. Functional relationships between denudation, relief, and uplift in large, mid-latitude drainage basins. American Journal of Science 268, 243–263.
Allmendinger, R.W., Jordan, T.E., Kay, S.M., Isacks, B.L., 1997. The evolution of the Altiplano-Puna Plateau of the Central Andes. Annual Review of Earth and Planetary Sciences 25, 139–174.
Anders, M.H., Gregory-Wodzicki, K.M., Spiegelman, M., 2002. A critical evaluation of late Tertiary accelerated uplift rates for the Eastern Cordillera, central Andes of Bolivia. Journal of Geology 110, 89–100.
Baby, P., Herail, G., Salinas, R., Sempere, T., 1992. Geometry and kinematic evolution of passive roof duplexes deduced from cross section balancing; example from the foreland thrust system of the southern Bolivian subandean zone. Tectonics 11, 523–536.
Baker, P.A., Rigsby, C.A., Seltzer, G.O., Fritz, S.C., Lowenstein, T.K., Bacher, N.P., Veliz, C., 2001a. Tropical climate changes at millennial and orbital timescales on the Bolivian Altiplano. Nature 409, 698–701.
Baker, P.A., Seltzer, G.O., Fritz, S.C., Dunbar, R.B., Grove, M.J., Tapia, P.M., Cross, S.L., Rowe, H.D., Broda, J.P., 2001b. The history of South American tropical precipitation for the past 25,000 years. Science 29, 640–643.
Balco, G., 2001. Topographic shielding and cosmogenic nuclide production rates over large areas. http://depts.washington.edu/cosmolab/math.html.
Barke, R., Lamb, S., 2006. Late Cenozoic uplift of the Eastern Cordillera, Bolivian Andes. Earth and Planetary Science Letters 249, 350–367.
Barnes, J.B., Ehlers, T., 2009. End member models for Andean Plateau uplift. Earth Science Reviews 97, 105–132.
Barnes, J.B., Pelletier, J.D., 2006. Latitudinal variation of denudation in the evolution of the Bolivian Andes. American Journal of Science 306, 1–31.
Barnes, J.B., Ehlers, T.A., McQuarrie, N., O'Sullivan, P.B., Pelletier, J.D., 2006. Variations in Eocene to recent erosion across the central Andean fold-thrust belt, northern Bolivia: implications for plateau evolution. Earth and Planetary Science Letters 248, 118–133.
Barnes, J.B., Ehlers, T.A., McQuarrie, N., O'Sullivan, P.B., Tawackoli, S., 2008. Thermochronometer record of central Andean plateau growth, Bolivia (19.5 S). Tectonics 27. doi:10.1029/2007TC002174.
Beaumont, C., Jamieson, R.A., Nguyen, M.H., Lee, B., 2001. Himalayan tectonics explained by extrusion of a low-viscosity crustal channel coupled to focused surface denudation. Nature 414, 738–742.
Benjamin, M.T., Johnson, N.M., Naeser, C.W., 1987. Recent rapid uplift in the Bolivian Andes; evidence from fission-track dating. Geology 15, 680–683.
Bierman, P., Steig, E.J., 1996. Estimating rates of denudation using cosmogenic isotope abundances in sediment. Earth Surface Processes and Landforms 21, 125–139.
Binford, M.W., Kolata, A.L., Brenner, M., Janusek, J.W., Seddon, M.T., Abbott, M., Curtis, J.H., 1997. Climate variation and the rise and fall of an Andean civilization. Quaternary Research 47, 235–248.
Blodgett, T.A., Isacks, B.L., 2007. Landslide erosion rate in the eastern Cordillera of Northern Bolivia. Earth Interactions 11, 1–30.
Bookhagen, B., Strecker, M.R., 2008. Orographic barriers, high-resolution TRMM rainfall, and relief variations along the eastern Andes. Geophysical Research Letters 35. doi:10.1029/2007GL032011.
Burbank, D.W., Blythe, A.E., Putkonen, J., Pratt-Sitaula, B., Gabet, E., Oskin, M., Barros, A., Ojha, T.P., 2003. Decoupling of erosion and precipitation in the Himalayas. Nature 426, 652–655.

Bush, M.B., Hansen, B.C.S., Rodbell, D.T., Seltzer, G.O., Young, K.R., Leon, B., Abbott, M.B., Silman, M.R., Gosling, W.D., 2005. A 17 000-year history of Andean climate and vegetation change from Laguna de Chochos, Peru. Journal of Quaternary Science 20, 703–714.

Clement, A.C., Seager, R., Cane, M.A., 2000. Suppression of El Nino during the mid-Holocene by changes in the Earth's orbit. Paleoceanography 15, 731–737.

Coppus, R., Imeson, A.C., 2002. Extreme events controlling erosion and sediment transport in a semi-arid sub-Andean valley. Earth Surface Processes and Landforms 27, 1365–1375.

Cross, S.L., Baker, P.A., Seltzer, G.O., Fritz, S.C., Dunbar, R.B., 2000. A new estimate of the Holocene lowstand level of Lake Titicaca, central Andes, and implications for tropical palaeohydrology. The Holocene 10, 21–32.

Dosseto, A., Bourdon, B., Gaillardet, J., Maurice-Bourgoin, L., Allegre, C.J., 2006. Weathering and transport of sediments in the Bolivian Andes; time constraints from uranium-series isotopes. Earth and Planetary Science Letters 248, 759–771.

Dunn, J., Hartshorn, K., Hartshorn, P., 1995. Structural styles and hydrocarbon potential of the sub-Andean thrust belt of southern Bolivia. AAPG Memoir 62, 523–543.

Ege, H., Sobel, E.R., Scheuber, E., Jacobshagen, V., 2007. Exhumation history of the southern Altiplano plateau (southern Bolivia) constrained by apatite fission-track thermochronology. Tectonics 26, TC1004. doi:10.1029/2005TC001869.

Ehlers, T., Poulsen, C.J., 2009. Influence of Andean uplift on climate and paleoaltimetry estimates. Earth and Planetary Science Letter 281, 238–248.

Ehlers, T.A., Chaudhri, T., Kumar, S., Fuller, C.W., Willett, S.D., Ketcham, R.A., Brandon, M.T., Belton, D.X., Kohn, B.P., Gleadow, A.J.W., Dunai, T.J., Fu, F.Q., 2005. Computational Tools for Low-Temperature Thermochronometer Interpretation. In: Reiners, P.W., Ehlers, T.A. (Eds.), Low-Temperature Thermochronology: Techniques, Interpretations, and Applications. Reviews in Mineralogy and Geochemistry. Mineralogical Society of America, Chantilly, VA, pp. 589–622.

Gabet, E.J., Burbank, D.W., Putkonen, J.K., Pratt-Sitaula, B.A., Ojha, T., 2004. Rainfall thresholds for landsliding in the Himalayas of Nepal. Geomorphology 63, 131–143.

Garreaud, R.D., 2000. Intraseasonal variability of moisture and rainfall over the South American Altiplano. Monthly Weather Review 128, 3337–3346.

Garreaud, R.D., Wallace, J.M., 1997. The diurnal march of convective cloudiness over the Americas. Monthly Weather Review 125, 3157–3171.

Garzione, C.N., Molnar, P., Libarkin, J., MacFadden, B., 2006. Rapid late Miocene rise of the Bolivian Altiplano: evidence for removal of mantle lithosphere. Earth and Planetary Science Letters 241, 543–556.

Gillis, R.J., Horton, B.K., Grove, M., 2006. Thermochronology, geochronology, and upper crustal structure of the Cordillera Real: implications for Cenozoic exhumation of the central Andean plateau. Tectonics 25. doi:10.1029/2005TC001887.

Graf, K., 1981. Palynological investigations of two post-glacial Peat Bogs near the Boundary of Bolivia and Peru. Journal of Biogeography 8, 353–368.

Guyot, J.L., Bourges, J., Hoorelbecke, R., Roche, M.A., Calle, H., Cortes, J., Guzman, M.C.B., 1988. Suspended Material Discharge from the Andes to the Amazonia along the Beni River, Bolivia. In: Bordas, M.P., Walling, D.E. (Eds.), Sediment Budgets, 174. IAHS Publication, pp. 443–451.

Guyot, J.L., Calle, H., Cortes, J., Pereira, M., 1990. Transport of suspended sediment and dissolved material from the Andes to the Rio de la Plata by the Bolivian tributaries of the Rio Paraguay (Rios Pilcomayo and Bermejo). Hydrologic Sciences Journal 35, 653–665.

Harden, C.P., 2006. Human impacts on headwater fluvial systems in the Northern and Central Andes. In: James, L.A., Marcus, W.A. (Eds.), Geomorphology, pp. 249–263.

Heisinger, B., Lal, D., Jull, A.J.T., Kubik, P., Ivy-Ochs, S., Knie, K., Nolte, E., 2002. Production of selected cosmogenic radionuclides by muons; 2, Capture of negative muons. Earth and Planetary Science Letters 200, 357–369.

Hilley, G.E., Strecker, M.R., 2004. Steady state erosion of critical Coulomb wedges with applications to Taiwan and the Himalaya. Journal of Geophysical Research 109. doi:10.1029/2002JB002284.

Hooke, R.L., 2000. On the history of humans as geomorphic agents. Geology 28, 843–846.

Horton, B.K., 1998. Sediment accumulation on top of the Andean orogenic wedge; Oligocene to late Miocene basins of the Eastern Cordillera, southern Bolivia. Geological Society of America Bulletin 110, 1174–1192.

Horton, B.K., 1999. Erosional control on the geometry and kinematics of thrust belt development in the central Andes. Tectonics 18, 1292–1304.

Hovius, N., 1998. Controls on sediment supply by large rivers. Special Publication—SEPM (Society for Sedimentary Geology) 59, 3–16.

Hovius, N., Stark, C.P., Chu, H.-T., Lin, J.-C., 2000. Supply and removal of sediment in a landslide-dominated mountain belt; Central Range, Taiwan. Journal of Geology 108, 73–89.

Insel, N., Poulsen, C.J., Ehlers, T.A., 2009. Influence of the Andes Mountains on South American moisture transport, convection, and precipitation. Climate Dynamics. doi:10.1007/s00382-009-0637-1.

IRIS, 2009. Incorporated Research Institutions for Seismology. http://www.iris.edu.

Isacks, B.L., 1988. Uplift of the Central Andean plateau and bending of the Bolivian Orocline. Journal of Geophysical Research 93, 3211–3231.

Jordan, T.E., Reynolds III, J.H., Erikson, J.P., 1997. Variability in Age of Initial Shortening and Uplift in the Central Andes. In: Ruddiman, W.F. (Ed.), Tectonic uplift and climate change. Plenum Press, New York, pp. 41–61.

Kirchner, J.W., Finkel, R.C., Riebe, C.S., Granger, D.E., Clayton, J.L., King, J.G., Megahan, W.F., 2001. Mountain erosion over 10 yr, 10 k.y., and 10 m.y. time scales. Geology 29, 591–594.

Kley, J., Monaldi, C.R., 1998. Tectonic shortening and crustal thickness in the Central Andes; how good is the correlation? Geology 26, 723–726.

Kley, J., Gangui, A.H., Krueger, D., 1996. Basement-Involved Blind Thrusting in the Eastern Cordillera Oriental, Southern Bolivia; Evidence from Cross-Sectional Balancing, Gravimetric and Magnetotelluric data. In: Dewey, J.F., Lamb, S.H. (Eds.), Geodynamics of the Andes. Elsevier, Amsterdam, pp. 171–184.

Lamb, S., 2000. Active deformation in the Bolivian Andes, South America. Journal of Geophysical Research, B, Solid Earth and Planets 105, 25,627–25,653.

Lenters, J.D., Cook, K.H., 1995. Simulation and diagnosis of the regional summertime precipitation climatology of South America. Journal of Climate 8, 2988–3005.

Leturmy, P., Mugnier, J.L., Vinour, P., Baby, P., Colletta, B., Chabron, E., 2000. Piggyback basin development above a thin-skinned thrust belt with two detachment levels as a function of interactions between tectonic and superficial mass transfer; the case of the Subandean Zone (Bolivia). Tectonophysics 320, 45–67.

Masek, J.G., Isacks, B.L., Gubbels, T.L., Fielding, E.J., 1994. Erosion and tectonics at the margins of continental plateaus. Journal of Geophysical Research 99, 13,941–13,956.

McQuarrie, N., 2002. The kinematic history of the central Andean fold-thrust belt, Bolivia; implications for building a high plateau. Geological Society of America Bulletin 114, 950–963.

McQuarrie, N., Davis, G.H., 2002. Crossing the several scales of strain-accomplishing mechanisms in the hinterland of the central Andean fold-thrust belt, Bolivia. Journal of Structural Geology 24, 1587–1602.

McQuarrie, N., Barnes, J.B., Ehlers, T.A., 2008a. Geometric, kinematic, and erosional history of the central Andean Plateau, Bolivia (15–17). Tectonics 27. doi:10.1029/2006TC002054.

McQuarrie, N., Ehlers, T.A., Barnes, J.B., Meade, B.J., 2008b. Temporal variation in climate and tectonic coupling in the central Andes. Geology 36, 999–1002.

Montgomery, D.R., Brandon, M.T., 2002. Topographic controls on erosion rates in tectonically active mountain ranges. Earth and Planetary Science Letters 201, 481–489.

Montgomery, D.R., Balco, G., Willett, S.D., 2001. Climate, tectonics, and the morphology of the Andes. Geology 29, 579–582.

Moy, C.M., Seltzer, G.O., Rodbell, D.T., Anderson, D.M., 2002. Variability of El Nino/southern Oscillation activity at millenial timescales during the Holocene epoch. Nature 420, 162–165.

Mulch, A., Uba, C., Strecker, M.R., Schoenberg, R., Chamberlain, C.P., 2010. Late Miocene climate variability and surface elevation in the central Andes. Earth and Planetary Science Letter 290, 173–182.

Niemi, N.A., Oskin, M., Burbank, D.W., Heimsath, A.M., Gabet, E.J., 2005. Effects of bedrock landslides on cosmogenically determined erosion rates. Earth and Planetary Science Letters 237, 480–498.

Nishiizumi, K., Imamura, M., Caffee, M.W., Southon, J.R., Finkel, R.C., McAninch, J., 2007. Absolute calibration of 10Be AMS standards. Nuclear Instruments and Methods in Physics Research B258, 403–413.

Oncken, O., Hindle, D., Kley, J., Elger, K., Victor, P., Schemmann, K., 2006. Deformation of the central Andean upper plate system—facts, fiction, and constraints for plateau models. In: Oncken, O., Chong, G., Franz, G., Giese, P., Gotze, H.-J., Ramos, V.A., Strecker, M.R., Wigger, P. (Eds.), The Andes: Active Subduction Orogeny. Frontiers in Earth Sciences. Springer-Verlag, Berlin, pp. 3–27.

Paduano, G.M., Bush, M.B., Baker, P.A., Fritz, S.C., Seltzer, G.O., 2003. A vegetation and fire history of Lake Titicaca since the last glacial maximum. In: Seltzer, G.O., Rodbell, D.T., Wright, H.E. (Eds.), Palaeogeography, Palaeoclimatology, Palaeoecology, pp. 259–279.

Pazzaglia, F.J., Brandon, M.T., 2001. A fluvial record of long-term steady-state uplift and erosion across the Cascadia forearc high, western Washington State. American Journal of Science 301, 385–431.

Peterson, T.C., Vose, R.S., 1997. An overview of the Global Historical Climatology Network Temperature database. Bulletin of the American Meteorological Society 78, 2837–2849.

Pinet, P., Souriau, M., 1988. Continental erosion and large-scale relief. Tectonics 7, 563–582.

Reiners, P.W., Ehlers, T.A., Mitchell, S.G., Montgomery, D.R., 2003. Coupled spatial variations in precipitation and long-term erosion rates across the Washington Cascades. Nature 426, 645–647.

Riebe, C., Kirchner, J., Granger, D., Finkel, R., 2001. Minimal climatic control on erosion rates in the Sierra Nevada, California. Geology 29, 447–450.

Rollins, H.B., Richardson III, J.B., Sandweiss, D.H., 1986. The birth of El Nino: geoarchaeological evidence and implications. Geoarchaeology 1, 3–15.

Rowe, H., Dunbar, R., Mucciarnone, D.A., Seltzer, G.O., Baker, P.A., Fritz, S., 2002. Insolation, moisture balance and climate change on the South American Altiplano since the Last Glacial Maximum. Climate Change 52, 175–199.

Safran, E.B., Bierman, P.R., Aalto, R., Dunne, T., Whipple, K.X., Caffee, M.W., 2005. Erosion rates driven by channel network incision in the Bolivian Andes. In: Heimsath, A.M., Ehlers, T.A. (Eds.), Earth Surface Processes and Landforms, pp. 1007–1024.

Safran, E.B., Blythe, A., Thomas, D., 2006. Spatially variable exhumation rates in orogenic belts: an Andean example. Journal of Geology 114, 665–681.

Sandweiss, D.H., Richardson III, J.B., Reitz, E.J., Rollins, H.B., Maasch, K., 1996. Geoarchaelogical evidence from Peru for a 5000 years B.P. onset of El Nino. Science 273, 1531–1533.

Schaller, M., Ehlers, T., 2006. Limits to quantifying climate driven changes in denudation rates with cosmogenic radionuclides. Earth and Planetary Science Letters 248, 138–152.

Schaller, M., von Blanckenburg, F., Hovius, N., Kubik, P.W., 2001. Large-scale erosion rates from in situ-produced cosmogenic nuclides in European river sediments. Earth and Planetary Science Letters 188, 441–458.

Schaller, M., von Blanckenburg, F., Veldkamp, A., Tebbens, L.A., Hovius, N., Kubik, P.W., 2002. A 30 000 yr record of erosion rates from cosmogenic (super 10) Be in middle European river terraces. Earth and Planetary Science Letters 204, 307–320.

Sempere, T., 1995. Phanerozoic evolution of Bolivia and adjacent regions. In: Tankard, A.J., et al. (Ed.), Petroleum basins of South America: American Association of Petreleum Geologists Memoir, 62, pp. 511–522.

Sempere, T., Herail, G., Oller, J., Baby, P., Barrios, L., Marocco, R., Laubacher, G., Olivier, R.A., Vatin-Perignon, N., 1990. The Altiplano; a province of intermontane foreland basins related to crustal shortening in the Bolivian Orocline area, Symposium international; Geodynamique andine; resumes des communications—International symposium; Andean geodynamics; abstracts. Editions de l'Office de la Recherche Scientifique et Technique d'Outre-mer, Paris, pp. 167–170.

Sempere, T., Butler, R., Richards, D., Marshall, L., Sharp, W., Swisher, C., 1997. Stratigraphy and chronology of Upper Cretaceous–lower Paleogene strata in Bolivia and Northwest Argentina. GSA Bulletin 109, 709–727.

Servant, M., Servant-Vildary, S., 2003. Holocene precipitation and atmospheric changes inferred from river paleowetlands in the Bolivian Andes. Palaeogeography, Palaeoclimatology, Palaeoecology 194, 187–206.

Servant, M., Fontes, J.-C., Rieu, M., Saliege, J.F., 1981. Holocene arid episodes in southwestern Amazonia. Comptes Rendus De L Academie Des Sciences Serie II 292, 1295–1297.

Smolders, A.J.P., Guerrero Hiza, M.A., Van der Velde, G., Roelofs, J.G.M., 2002. Dynmics of discharge, sediment transport, heavy metal pollution and Sabalo (*Prochilodus lineatus*) catches in the Lower Pilcomayo River (Bolivia). River Research and Applications 18, 415–427.

Stock, G.M., Frankel, K.L., Ehlers, T.A., Schaller, M., Briggs, S.M., Finkel, R.C., 2009. Spatial and temporal variations in erosion from multiple geochronometers: Wasatch Mountains, Utah, USA. GSA Lithosphere 1, 34–40. doi:10.1130/L15.1.

Stone, J.O., 2000. Air pressure and cosmogenic isotope production. Journal of Geophysical Research 105, 23,753–23,759.

Summerfield, M.A., Hulton, N.J., 1994. Natural controls of fluvial denudation rates in major world drainage basins. Journal of Geophysical Research 99, 13,871–13,883.

Uba, C., Kley, J., Strecker, M.R., Schmitt, A.K., 2009. Unsteady evolution of the Bolivian Subandean thrust belt: the role of enhanced erosion and clastic wedge progradation. Earth and Planetary Science Letter 281, 134–146.

von Blanckenburg, F., 2005. The control mechanisms of erosion and weathering at basin scale from cosmogenic nuclides in river sediment. Earth and Planetary Science Letters 237, 462–479.

von Blanckenburg, F., Belshaw, N.S., O'Nions, R.K., 1996. Separation of (super 9) Be and cosmogenic (super 10) Be from environmental materials and SIMS isotope dilution analysis. Chemical Geology 129, 93–99.

Vuille, M., 1999. Atmospheric circulation over the Bolivian Altiplano during dry and wet periods and extreme phases of the Southern Oscillation. International Journal of Climatology 19, 1579–1600.

Wilkinson, B.H., McElroy, B.J., 2007. The impact of humans on continental erosion and sedimentation. Geological Society of America Bulletin 119, 140–156.

Willett, S., 1999. Orogeny and orography; the effects of erosion on the structure of mountain belts. Journal of Geophysical Research 104, 28957–28982.

Wittman, H., Von Blanckenburg, F., Guyot, J.L., L, M., Kubik, P.W., 2009. From source to sink: preserving the cosmogenic 10Be-derived denduation rate signal of the Bolivian Andes in sediment of the Beni and marmore foreland basins. Earth and Planetary Science Letter 288, 463–474.

Wittmann, H., Blanckenburg, F.v., 2009. Cosmogenic nuclide budgeting of floodplain sediment transfer. Geomorphology 109, 246–256.

Yanites, B., Tucker, G.E., Anderson, R.S., 2009. Numerical and analytical models of cosmogenic radionuclide dynamics in landslide-dominated drainage basins. Journal of Geophysical Research 114. doi:10.1029/2008JF001088.